EFFECT OF HYDROGEN ON FATIGUE PROPERTIES OF Ni-Cr-Mo STEEL (JIS-SNCM439)[1]

Hiroki Yano[2]
Saburo Matsuoka[3]
Yukitaka Murakami[4]
Françoise Barbier[5]
Jader Ferreira Furtado Filho[6]

Abstract

The Ni-Cr-Mo steel (JIS-SNCM439) is being considered as a candidate material for the hydrogen storage buffer in 70 MPa hydrogen stations. In the present work, the effect of hydrogen on fatigue properties of JIS-SNCM439 was quantified with tension-compression fatigue tests carried out at frequencies of 0.2, 2, 20 and 500 Hz. Smooth specimens and specimens containing a small artificial hole were tested at room temperature in laboratory air. The fatigue specimens were charged with hydrogen either by the 100 MPa hydrogen gas exposure method or by the immersion method into ammonium thiocyanate solution. The fatigue life of the H_2-charged specimens decreased in comparison with the uncharged specimens. For specimens containing a small hole, it was observed an acceleration of fatigue crack growth rate, da/dN, for the H_2-charged specimens when compared to the uncharged samples. However, it was verified that this acceleration rate has reached an upper limit of approximately 10 times the acceleration rate found for uncharged specimens. In the case of smooth specimens, the fracture has originated off a cluster of Al_2O_3 inclusions. The square root of the projected area of the inclusion model, $\sqrt{area}$ parameter model, was applied to predict the fatigue strength of uncharged and hydrogen-charged specimens.

Key words: Fatigue; Hydrogen; Ni-Cr-Mo steel; $\sqrt{area}$ Parameter model.

EFFEITO DO HIDROGÊNIO NAS PROPRIEDADES DE FADIGA DO AÇO NI-CR-MO (JIS-SNCM439)

Resumo

O aço Ni-Cr-Mo (JIS-SNCM439) esta sendo considerado como um candidato potencial para a fabricação dos tanques para armazenar hidrogênio em altas pressoes, por exemplo 70 MPa, que serão utilizados nos futuros postos de abastecimento a hidrogenio de carros movidos à pilha-combustivel. Neste trabalho, são quantificados os efeitos do hidrogenio nas propriedades de fadiga do aço JIS-SNCM439. Os ensaios de fadiga foram realizados ao ar de laboratorio, sob tensão-compressão, nas frequencias de 0.2, 2, 20 e 500 Hz. Os corpos de provas utilizados são do tipo liso ou com furos superficiais calibrados. Antes dos testes as amostras foram saturadas com hidrogenio pelos metodos de exposiçao ao gas sob pressão de 100 MPa ou por imersão em soluçao eletrolitica. A vida em fadiga das amostradas carregadas com hidrogenio diminuiu em relaçao às amostras não-saturadas com hidrogênio. Nas amostras contendo um pequeno furo calibrado, observou-se uma aceleraçao da taxa de propagaçao da trinca de fadiga, d*a*/d*N*, para as amostras carregadas com H_2 quando comparadas com as amostras nao-carregadas. Entretando, verificou-se que esta taxa de aceleraçao alcançou um limite superior de propagaçao, equivalente à aproximadamente 10 vezes a taxa de propagaçao das amostras nao-carregadas com hidrogenio. No caso dos corpos de prova lisos, a fratura por fadiga iniciou-se num grupo de inclusoes de Al_2O_3. Em seguida, foi utilizado o modelo da raiz quadrada da area projetada da inclusao, « $\sqrt{area}$ parameter model », para se prever o limite de resistencia em fadiga das amostras testadas e que foram carregadas ou não com o hidrogenio.

Palavras-chave: Fadiga; Hidrogênio; *Aço* Ni-Cr-Mo.

[1] *Technical contribution to 65th ABM Annual Congress, July, 26th to 30h, 2010, Rio de Janeiro, RJ, Brazil.*

[2] *M. Sc student, Graduate School of Engineering, Kyushu University, Fukuoka, Japan.*
[3] *Professor Department of Mechanical Engineering Science, Kyushu University / National Institute of Advanced Industrial Science and Technology (AIST), Fukuoka, Japan.*
[4] *Vice-Chancellor and Trustee, Prof. Dep. Mechanical Engineering Science, Kyushu University / AIST, Japan.*
[5] *Air Liquide R & D, Hydrogen Energy Domain Director, Centre de Recherche Claude-Delorme (CRCD), Les Loges-en-Josas, France.*
[6] *Member of ABM, Air Liquide R & D, International Expert R&D-Physical Metallurgy, CRCD, Les Loges-en-Josas, France / Special Appointment Professor Department of Mechanical Engineering Science, Kyushu University, Fukuoka, Japan.*

1 INTRODUCTION

The storage cylinder of a hydrogen station is one of the major components of hydrogen supply system to fuel cell vehicles (FCVs). In Japan, following the demonstration of the 35 MPa hydrogen station (35 MPa HS), it has started the demonstration project of 70 MPa hydrogen station (70 MPa HS) aiming at to increase the useful range in kilometres of FCVs.[1] In the first program was used Cr-Mo steel JIS-SNCM435, but for the 70 MPa HS is envisaged to use instead the Ni-Cr-Mo steel JIS-SNCM439 due to its better quench hardenability. This mechanical property is an important requirement as we have to consider that the design of the storage cylinder of 70 MPa HS will require thicker thickness compared to that of 35 MPa HS.

Storage cylinders of hydrogen stations (HS) are vessels designed to store high pressure hydrogen gas. In such conditions the steel used for the manufacturing of the storage cylinder will be exposed to high pressure hydrogen gas directly and hydrogen will diffuse inside the material inevitably. Another important consideration is that the storage cylinder of HS will be subjected to a cyclic stress loading pattern as hydrogen gas pressure changes due to the supplying of hydrogen gas to FCVs.

Tanaka et al.[2] studied the Cr-Mo low alloy steel JIS-SCM435 used in the 35 MPa HS and showed that although crack growth rate is accelerated by hydrogen, there is an upper limit for the crack growth acceleration rate. They verified that this upper limit of crack growth acceleration by hydrogen is approximately 30 times higher in comparison to the crack growth rate without hydrogen. The testing conditions they have employed: R (stress ratio) = -1 (fully reversed), f (test frequency) = 0.2 ~ 20 Hz, at room temperature in laboratory air.

In the case of the Ni-Cr-Mo low alloy steel JIS-SNCM439 there is no available technical information on how high pressure hydrogen will affect the fatigue properties of this steel. In order to lay down the guidelines for the storage cylinder design and safety assessment there is a need of clarifying this point. Therefore, the objective of this study is to examine the effects of hydrogen on fatigue properties of the Ni-Cr-Mo low alloy steel JIS-SNCM439.

2 MATERIAL AND EXPERIMENTAL METHODS

2.1 Material and Fatigue Specimens

The material used in this study was the Ni-Cr-Mo low alloy steel according to the JIS-SNCM439 Japanese standard specification. The composition and mechanical properties of this steel are given in Tables 1 and 2, respectively. The steel is a high carbon, quenched and tempered forging steel that has nominal yield strength of 754 MPa and a quenched and tempered martensite microstructure. This steel has an average Vickers hardness of 292, which was obtained from 29 measurements with the applied load of 294 N.

Fatigue test specimens were machined from a 70 MPa HS storage cylinder prototype with dimensions given in Figure 1. The fatigue specimens were taken from the cylinder thickness with its axial direction coincident with the circumferential direction of the storage cylinder shown in Figure 2. Two types of round fatigue samples have been used: smooth specimens as shown in Figure 3(a) were employed to obtain S-N fatigue properties, and specimens containing small artificial defect (calibrated hole) (Figure 3(b)) were used to study crack propagation. The artificial hole was drilled into the centre surface of the specimens with the purpose to

start a fatigue crack. The hole dimensions were 100 µm in diameter and 100 µm deep or 300 µm in diameter and 300 µm deep as detailed in Figure 3(c).[3]

Prior to fatigue testing and hydrogen pre-charging all specimens were given the same surface finishing up to #2000 emery paper.

Table 1. Chemical composition of SNCM439 steel (wt %)

	C	Si	Mn	P	S	Ni	Cr	Mo	*HV*
JIS-SNCM439	0.43	0.27	0.82	0.005	0.002	1.95	0.91	0.23	292

Table 2. Mechanical Properties of SNCM439

Yield Stress σ_Y (MPa)	Tensile Strength σ_B (MPa)	Elongation at Fracture δ (%)	Reduction of area ϕ (%)
754	927	17.1	55.3

δ: elongation at fracture; ϕ: reduction of area; $\sigma_B=\sigma_{UTS}$; $\sigma_Y=\sigma_{YS}$

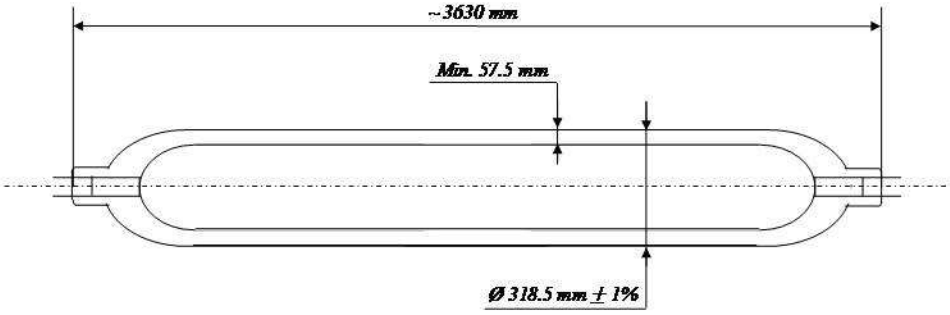

Figure 1. Shape and dimensions of the high pressure hydrogen tank prototype.

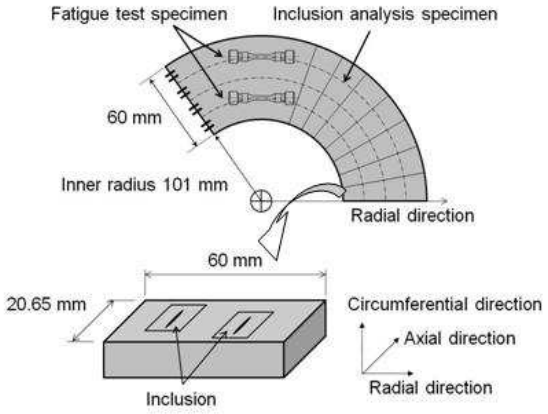

Figure 2. Specimen orientation.

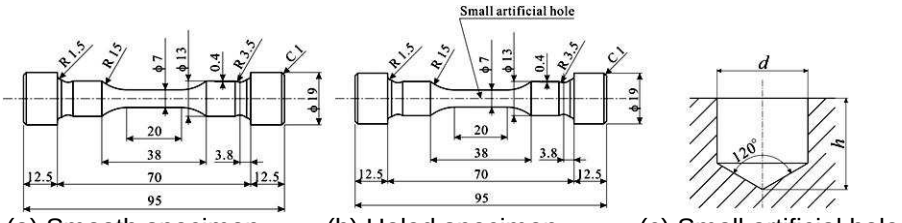

(a) Smooth specimen (b) Holed specimen (c) Small artificial hole

Figure 3. Shape and dimensions of fatigue test specimen.

2.2 Hydrogen Charging and Hydrogen Content Measurement

Kim et al.[4] studied the hydrogen permeation properties of JIS-SNCM439 steel with σ_{UTS} = 981 MPa and found the diffusion coefficient D ≈ 1.95 × 10-10 m2/s. Using this D value for the steel used in the present work and applying the Fick's second law,[5] we found that our fatigue specimens should be saturated by hydrogen after around 3 hours of hydrogen charging. This charging time has been used as a time reference to adjust our hydrogen charging conditions to attain the expected saturation levels of hydrogen for the buffer in a hydrogen station.

Hydrogen charging was carried out by exposing specimens to high pressure hydrogen gas at 100 MPa pressure and 85 ℃ for 200 h (gas charging) or by immersing specimens into ammonium thiocyanate solution (with 20 wt% of CH_4NCS) held at 40 ℃ for 24 h (immersion charging).

Since fatigue tests of hydrogen charged specimens were performed at room temperature in laboratory air, hydrogen is expected to diffuse out of the specimens during the tests. Therefore it is important to estimate the decrease in hydrogen content of the specimens during the fatigue test. To carry out this task, circular disk samples with thickness of 2 mm were cut out at given time intervals from hydrogen-charged round bar samples with dimensions of ϕ 6.4 × 25 mm either by gas charging or immersion charging. Similar disk samples were also cut out from the fatigue test specimens immediately after finishing the test.

Hydrogen content of the disk samples was measured using thermal desorption spectrometry (TDS). The basic principle of this method is that the sample is heated in a controlled manner and the quantity of hydrogen released is monitored using a mass spectrometer. The hydrogen-charged sample was heated up to 600℃ at a heating rate of 0.5℃/s. The diffusible peak 1 of h ydrogen content discharged between room temperature and 300℃ was used in this study to quantify the hydrogen content of the pre-charged sample.[6] The relationship between hydrogen content (C_H) of samples and elapsed time after hydrogen charging was approximated by using the least-square method.

2.3 Inclusion Rating and the $\sqrt{area}$ Parameter Model

Inclusions play an important role in the endurance life of steel parts subject to fatigue because they can act as crack-like defects and start the fatigue crack propagation process. The inclusions effect will be more pronounced if they are located at the steel surface. Taking this fact into consideration, Murakami[7,8] proposed a model where the inclusion size and location is considered for the calculation of the fatigue limit. He proposed that the fatigue limit (σ_W) can be correlated to the $\sqrt{area}$ parameter, e.g., the square root of the projected area of the inclusion, which can be regarded as a characteristic dimension of the defect or inclusion.

$$\sigma_w = \frac{\alpha(HV + 120)}{(\sqrt{area})^{1/6}} \quad (1)$$

where $\sqrt{area}$ is the square root of the projected area of initial defect (μm), σ_w is the fatigue limit, HV is the Vickers hardness and α is a constant number. For internal crack, α = 1.56, and for surface crack, α = 1.43.

As described in Equation 1 the rating of $\sqrt{area}$ parameter is a key variable to the model application. Murakami has developed a methodology of doing so based on the Gumbel distribution of extreme values. The aim of this statistical analysis is to quantify the maximum length of inclusions (l_{max}) or the maximum $\sqrt{area}$ of the projected inclusion. To carry out the analysis of statistics of extreme distributions, metallographic samples were prepared. The inspection area (S0) was chosen as 1239 mm^2 and the number of inspections (n) equal to 15. Details of the methodology are explained elsewhere.[8]

Inclusions were observed with the scanning electron microscope (SEM) and identified with energy dispersive X-ray analyzer (EDX) installed in the SEM.

2.4 Fatigue Tests

Fatigue tests were performed at room temperature, in laboratory air, using servo-hydraulic fatigue machine under load control following a sine wave function. The stress ratio (R) was R = -1 (fully reversed) and the test frequencies (f) were f = 0.2, 2, 20 and 500 Hz. The frequency of 500 Hz was chosen in order to verify the effect of hydrogen on the fatigue limit at 10^7 cycles.

For specimens with a drilled calibrated hole with dimensions of 300 µm in diameter and 300 µm deep a fatigue precrack with a length of 2a ≈ 600 µm was introduced. This procedure was not used for specimens with drilled holes with dimensions of 100 µm in diameter and 100 µm deep. Once the fatigue crack has reached the specimen surface it was measured by using the plastic replica method. The crack propagation rate was determined by using the secant method as proposed in Shiratori et al.[9] and the ASTM E647 standard.[10]

3 RESULTS AND DISCUSSION

3.1 Hydrogen Release Properties

Figure 4 shows the hydrogen content (C_H) of charged samples measured by the TDS technique after selected elapsed hours for the gas-charging and immersion-charging methods. In both cases hydrogen content decreased monotonically with elapsed time after hydrogen charging. Concerning gas-charged samples, almost all hydrogen was released within 70 h. This data has been used to guide the choice of test frequency for fatigue tests running around the fatigue limit at 10^7 cycles to failure. For instance, using the test frequency of 500 Hz the expected fatigue test duration can be reached around 13 hours.

The relationship between hydrogen content (C_H) of samples and elapsed time after hydrogen charging was fitted by the following equations:

a) gas-charged samples

$$C_H = 0.33\exp(-0.05t) \quad (2)$$

b) immersion-charged samples

$$C_H = 0.25\exp(-0.09t) \quad (3)$$

Considering the charging protocols used in this work, gas-charged samples presented higher values of saturated hydrogen content (C_H) in comparison to the immersion charging method. Based on these TDS measurements, the hydrogen content of fatigue precharged samples at the beginning of the fatigue test was considered as 0.33 wppm for gas-charged samples and 0.25 wppm for immersion-charged samples.

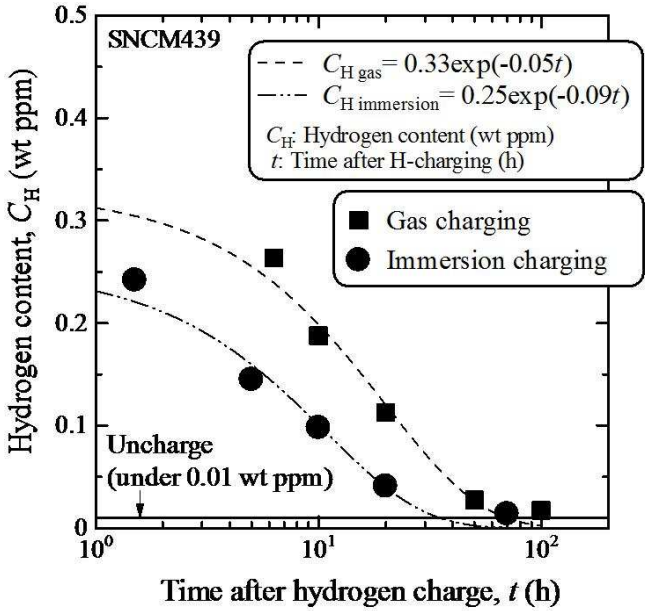

Figure 4. Decrease in hydrogen content, CH, after hydrogen charge.

3.2 Inclusion Identification and Rating

MnS and Al_2O_3 inclusions were identified by the EDX detector during the SEM observations and they are shown in Figure 5. Sulphide inclusions are typically elongated as a result of the forging process. On the other hand, the alumina inclusions were grouped in clusters. Average widths of inclusions of maximum longitudinal length, 2c, on each inspecting standard areas were 12.2 µm for MnS inclusions and 15.6 µm for clusters of Al_2O_3 inclusions.

In Figure 6 it is shown the statistics of extreme distributions of inclusions of maximum longitudinal length, l_{max}, and equivalent to the $\sqrt{area}$, plotted against the reduced variate y and the cumulative distribution function F. The maximum length of inclusions, lmax, of MnS inclusions varied in the range of 81.9 ~ 221.6 µm and for the cluster of Al_2O_3 inclusions was in the range of 64.6 ~ 213.6 µm.

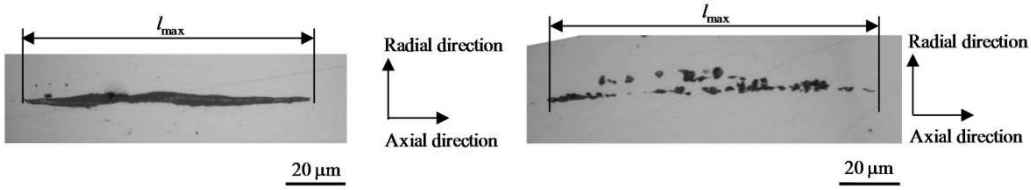

(a) MnS inclusion (b) Cluster of Al2O3 inclusion

Figure 5. Inclusions on transverse section.

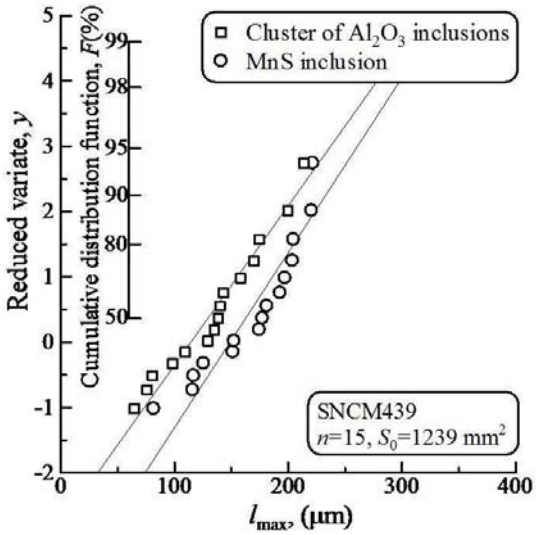

Figure 6. Statistics of extreme distributions of inclusions on transverse section. l_{max} or $\sqrt{area}$ is the maximum size of inclusions found in the inspected areas.

3.3 Effect of Hydrogen on S-N Properties

The fatigue testing results are shown in Table 3. Six out of the seven holed specimens fractured from the small artificial hole or precrack. Only one holed specimen that was immersion-charged and had one small artificial hole of 100 μm in diameter and 100 μm deep fractured from a cluster of Al_2O_3 inclusions. All seven uncharged smooth specimens and all eight hydrogen-charged smooth specimens fractured from cluster of Al_2O_3 inclusions. In Table 3 $\sqrt{area}$ is the square root of projected area of the fracture origin.

Hydrogen content of the specimens at the beginning and the end of the test were calculated by substituting the time after hydrogen charging to Equations (2) and (3). In Table 3 hydrogen content measured after the fatigue tests are indicated in parenthesis.

Hydrogen content of materials in thermal equilibrium, C_H, can be expressed by the Sieverts law:[5,11]

$$C_H = \sqrt{p}\exp(-1000/T) \qquad (4)$$

where p is hydrogen gas pressure (MPa) and T is temperature (K). The saturated hydrogen content under the condition that T=358 K, and p=100 MPa, C_{H100}, is estimated from the equation in Figure 2. At t=0, the saturated hydrogen content, C_{H100}, is C_{H100} ≈ 0.33 ppm. In general, T=358 K is regarded as the maximum allowable temperature of hydrogen gas in storage vessels for FCVs. If T=358 K is also the maximum allowable temperature, the saturated hydrogen content at p=70 MPa, C_{H70}, can be estimated by:

$$C_H = \sqrt{70/100}\,xC_{H100} = 0.28\,ppm \qquad (5)$$

This value is close to the maximum hydrogen content in this study.

Table 3. Results of fatigue tests

Specimen	Hydrogen Charge	σ_a (MPa)	R	f (Hz)	N_f(cycles)	Fracture Origin	$\sqrt{area}$ (μm)	Hydrogen Content (wt ppm)	Symbol
Hole or Hole + Precrack	Uncharge	500	-1	20	56,000	Hole	92.5	under 0.01^{++}	◇
	Uncharge	400	-1	20	69,500	Precrack	377.2	under 0.01^{+}	
	Immersion	500	-1	20	43,391	Inclusion(S^{*})	-	$0.15^{+}\rightarrow0.10^{+}$ (0.08^{++})	◈
	Immersion	400	-1	2	39,500	Precrack	367.8	$0.16^{+}\rightarrow0.07^{+}$ (0.07^{++})	◭
	Immersion	400	-1	0.2	-	Precrack	363.5	$0.16^{+}\rightarrow0.04^{+}$ (0.02^{++})	▽
	Gas	400	-1	2	21,500	Precrack	374.7	$0.24^{+}\rightarrow0.12^{+}$ (0.30^{++})	▲
	Gas	400	-1	0.2	13,000	Precrack	374.1	$0.25^{+}\rightarrow0.08^{+}$ (0.29^{++})	▼
Smooth	Uncharge	550	-1	20	36,981	Inclusion(S^{*})	29.8	under 0.01^{+}	□
	Uncharge	500	-1	20	100,618	Inclusion(I^{**})	140.7	under 0.01^{+}	
	Uncharge	450	-1	20	219,689	Inclusion(S^{*})	37.2	under 0.01^{+}	
	Uncharge	400	-1	20	214,236	Inclusion(S^{*})	207.5	under 0.01^{+}	
	Uncharge	350	-1	20	419,815	Inclusion(S^{*})	207.1	under 0.01^{+}	
	Uncharge	300	-1	500	10^7(ran out)	-	-	under 0.01^{+}	○
	Uncharge	300	-1	500	10^7(ran out)	Inclusion(I^{**})	59.4	under 0.01^{+}	
	Gas	550	-1	20	40,510	Inclusion(S^{*})	39.5	$0.30^{+}\rightarrow0.26^{+}$ (0.22^{++})	■
	Gas	500	-1	20	84,719	Inclusion(S^{*})	24.3	$0.30^{+}\rightarrow0.25^{+}$ (0.11^{++})	
	Gas	450	-1	20	80,647	Inclusion(S^{*})	51.4	$0.30^{+}\rightarrow0.26^{+}$ (0.12^{++})	
	Gas	400	-1	20	5.6×10^6(ran out)	Inclusion(S^{*})	33.2	$0.30^{+}\rightarrow0.01^{+}$ (0.02^{++})	
	Gas	400	-1	500	564,108	Inclusion(I**)	109.4	$0.25^{+}\rightarrow0.24^{+}$ (0.11^{++})	●
	Gas	350	-1	500	10^7(ran out)	Inclusion(S^{*})	46.3	$0.25^{+}\rightarrow0.19^{+}$ (0.11^{++})	
	Gas	350	-1	500	10^7(ran out)	Inclusion(I**)	61.8	$0.24^{+}\rightarrow0.18^{+}$ (0.08^{++})	
	Gas	300	-1	500	10^7(ran out)	Inclusion(I**)	93.3	$0.24^{+}\rightarrow0.18^{+}$ (0.06^{++})	

*: Surface inclusion. $^{+}$: Calcurated values before and after testing.
**: Internal inclusion. $^{++}$: Measured values after testing.

Fatigue lives of hydrogen-charged specimens decrease in comparison with those of uncharged specimens. This behaviour does not dependent on the existence of a drilled hole (defect), and it has been observed even in the case of smooth specimens. However, fatigue limit obtained from tests performed at f = 500 Hz did not decrease with hydrogen (Figure 7).

Regarding the fatigue lives of holed specimens with a precrack of 2a ≈ 600 μm and tested at σ_a = 400 MPa (◇,◭,▲,▼), fatigue lives of the hydrogen-charged specimens (◭,▲,▼) decreased compared to that of the uncharged specimen (◇). In the case of smooth specimens, the shape and dimensions of fracture origins were not identical. Hence, effects of hydrogen in S-N properties of smooth specimens cannot be evaluated correctly on Figure 7. Under these circumstances, the effects of initial dimensions of fracture origins must be considered to measure the effects of hydrogen and will be explained in section 3.4.

In Figure 7 it is also plotted the S-N data of JIS-SNCM439 (HV 307 ~ 328, R = -1) from NIMS fatigue data sheet No. 25.[12] Though the Vickers hardness of JIS-SNCM439 tested by NIMS is about the same as that in this study, fatigue strength of JIS-SNCM439 tested by NIMS is higher than JIS-SNCM439 used in this study. The better fatigue resistance is linked to the origin of the fractured samples. In the case of JIS-SNCM439 tested by NIMS fracture has started at the sample surface, whereas JIS-SNCM439 samples used in this study fractured from a small artificial hole, precrack or inclusions.

ISSN 1516-392X

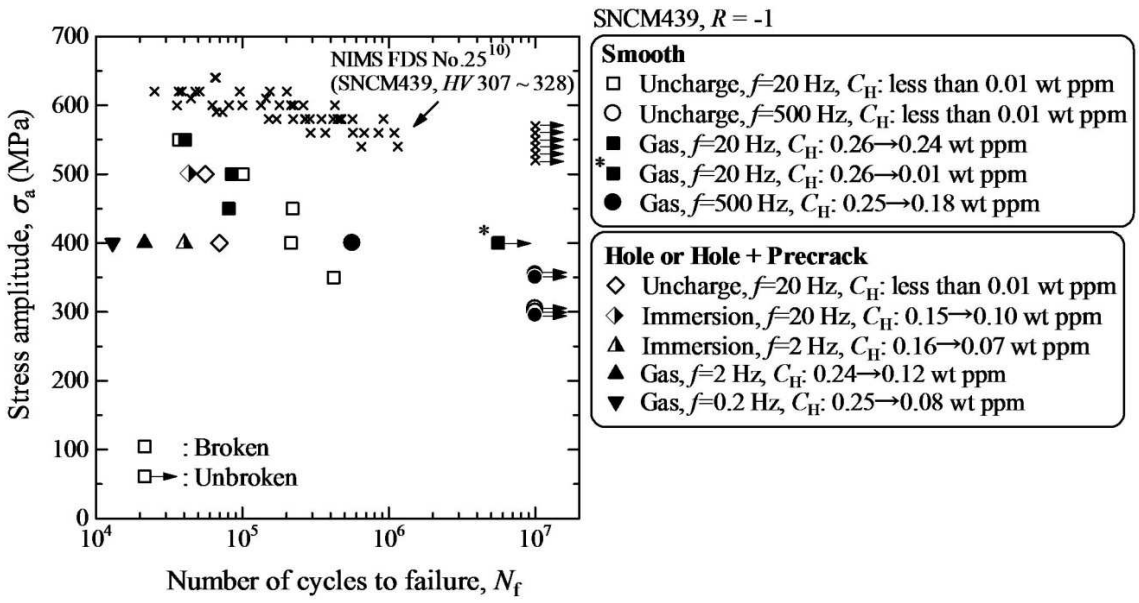

Figure 7. Effect of hydrogen and test frequency on S-N diagram.

Figure 8 shows examples of fracture origins of smooth specimens. According to the statistics of extreme distribution of inclusions shown in Figure 6, the maximum longitudinal length, l_{max}, of MnS inclusions was longer than that of clusters of Al_2O_3 inclusions. Despite this fact, the fatigue fracture origins were not MnS inclusions but only clusters of Al_2O_3 inclusions. According to Figure 6, the maximum length of clusters of Al_2O_3 inclusions was 64.6 ~ 213.6 μm long. In general, the dimension of spherical Al_2O_3 inclusions at internal fracture origin is less than about 30 μm in diameter.[13-15] The dimensions of Al_2O_3 clusters found in the material used for this study is larger in comparison with the spherical Al_2O_3.

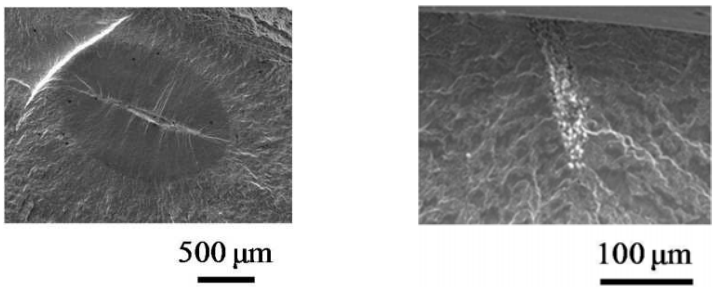

(a) Internal inclusion (Al2O3) (b) Surface inclusion (Al2O3)

Figure 8. Fracture origins of smooth specimen.

Some clusters of Al_2O_3 inclusions are located within the fracture surface as shown in Figure 8(a), but other clusters reached the specimen surface as shown in Figure 8(b). The dimensions of these inclusions, $\sqrt{area}$, were measured and shown in Table 3. Effective $\sqrt{area}$ is estimated as $\sqrt{area} \approx$ 10c, for the extremely shallow and long external defect (l ≥ 10c) shown in Figure 9(a) and for the extremely deep and thin external defect (l ≥ 5c) shown in Figure 9(b).[16] For the extremely long and thin internal defect (l ≥ 5c, 2l: long axis (length), 2c: short axis (width)) like Figure 8(a), the effective $\sqrt{area}$ is estimated as $\sqrt{area} \approx \sqrt{5\pi c}$, assuming a defect of approximately l ≈ 5c.[17]

According to this estimation method of effective $\sqrt{area}$, the reason the origins were not MnS inclusions but only clusters of Al_2O_3 inclusions can be explained on the basis that clusters of Al_2O_3 inclusions had wider width, 2c, when compared to MnS inclusions. As described in section 2.3, the average value of 2c, the width of defect, was 15.6 μm for clusters of Al_2O_3 inclusions and 12.2 μm for MnS inclusions. Thus, the average $\sqrt{area}$ of clusters of Al_2O_3 inclusions is larger compared to that of MnS inclusions. Additionally, the reason that the immersion-charged holed specimen (hole size: 100 μm in diameter and 100 μm deep) fractured from a cluster of Al_2O_3 inclusions can be explained by the $\sqrt{area}$ of the cluster of Al_2O_3 inclusions at fracture origin being larger than that of the small artificial hole. Unfortunately the $\sqrt{area}$ of the Al_2O_3 inclusions cluster at fracture origin could not be measured because the fracture surface of that specimen was crashed. However, five smooth specimens had larger $\sqrt{area}$ ($\sqrt{area}$ ≈ 93.3 ~ 207.5 μm) compared with the of the small artificial hole ($\sqrt{area}$ ≈ 92.5 μm) and shown in Table 3. This could explain why the fatigue crack has its fracture origin in the Al_2O_3 inclusions cluster.

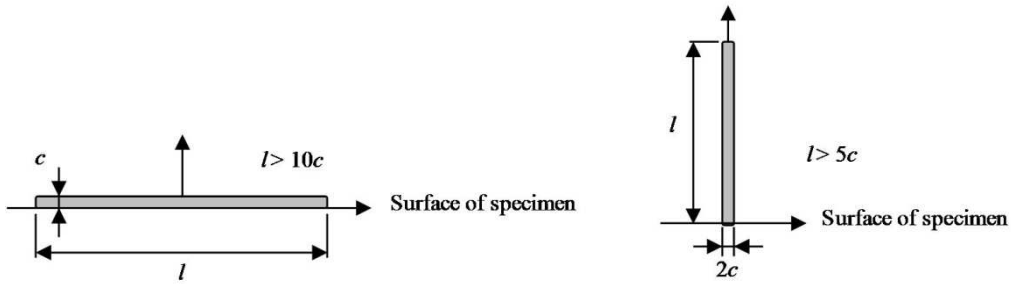

(a) Extremely shallow and long external crack (b) Extremely deep external crack

(effective $\sqrt{area} \approx \sqrt{10}c$) (effective $\sqrt{area} \approx 10c$)

Figure 9. Effective $\sqrt{area}$ for extremely long and thin cracks.

3.3 Fatigue Crack Growth Rate

Figure 10 shows the relationship between the fatigue crack growth rate, da/dN, and the stress intensity factor range, ΔK. The ΔK is given by the relationship: [9]

$$\Delta K = K_{max} - K_{min} = F\Delta\sigma\sqrt{\pi a} \qquad (6)$$

where F is nondimensional stress intensity factor, Δσ is the stress amplitude and a is the crack length.

The fatigue crack propagation rates (da/dN) of hydrogen-charged specimens were accelerated by hydrogen relative to that of uncharged specimen. The acceleration level of gas-charged specimen (hydrogen content during the test, C_H = 0.25 ~ 0.08 wppm) was higher compared to that of immersion-charged specimen (C_H = 0.16 ~ 0.04 wppm). This result suggests that the hydrogen-induced crack growth acceleration depends on the hydrogen content of the material.

On the other hand, in the case of gas-charged specimen, da/dN tested at f = 2 Hz (C_H = 0.24 ~ 0.12 wppm) coincides with da/dN tested at f = 0.2 Hz (C_H = 0.25 ~ 0.08

wppm) at around ΔK = 20 $MPa\sqrt{m}$. It seems that there is an upper limit for the hydrogen-induced da/dN acceleration rate, as has been observed before by Tanaka et al. [2] in the case of JIS-SNCM435 steel. This upper limit of the da/dN acceleration rate is approximately 10 times higher than da/dN of uncharged specimen.

Fatigue crack propagation is generally expressed by the expression: [18, 19]

$$da/dN = C\Delta K^{m} \qquad (7)$$

where C and m are constant numbers depending on material and stress ratio (R).

The C and m constants were calculated from the data given in Figure 10, by the least-square method. For uncharged specimens, C and m were calculated as $C_u \approx 3.60 \times 10^{-12}$ and m ≈ 2.52. For gas-charged specimens, the upper limit of the constant C is calculated as $C_{H(lim)} \approx 3.60 \times 10^{-11}$, considering the upper limit of the hydrogen-induced da/dN acceleration as 10 times.

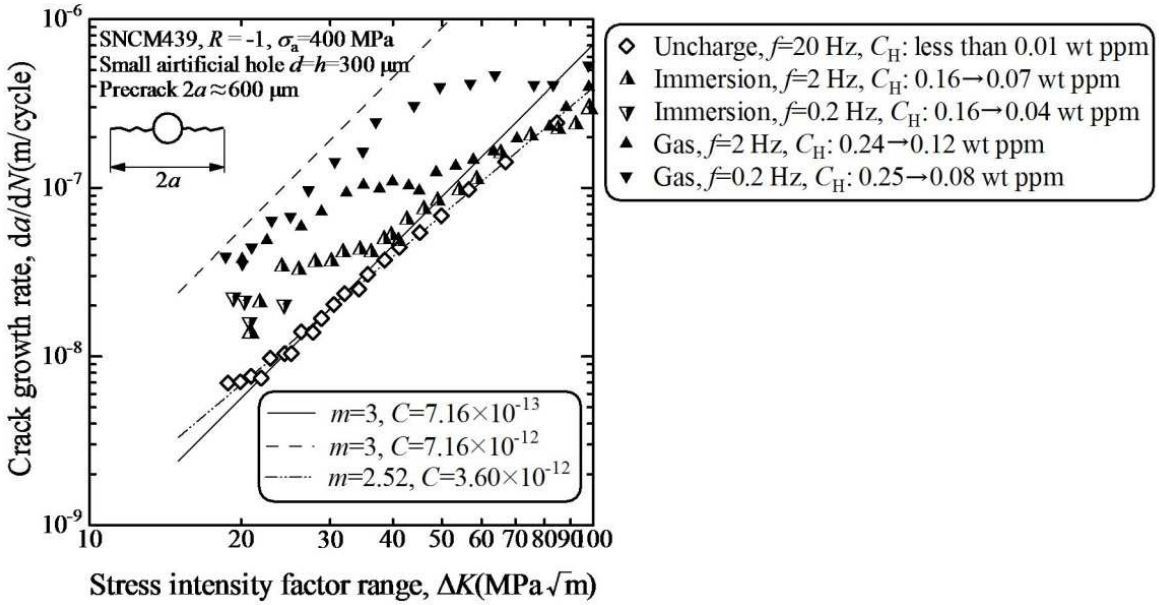

Figure 10. Relationship between crack growth rate, da/dN, and stress intensity factor range, ΔK.

3.4 Modified S-N Properties

As described in section 3.2, the effect of initial defect dimensions at fracture origins must be considered to evaluate the effect of hydrogen on S-N properties of smooth specimens. In order to eliminate the effects of initial defect dimension a modified S-N diagram[8] was constructed. The modified S-N diagram shows the relationship between the ratio between stress amplitude, σa (MPa), and estimated fatigue limit, σ_w (MPa), and number of cycles to failure, N_f. The estimated fatigue limit, σ_w, was calculated using Equation (1). [15, 20-21]

Figure 11 shows the modified S-N diagram constructed by using $\sqrt{area}$ shown in Table 3. For specimens that fractured from internal inclusion, α = 1.56 was substituted and α = 1.43 was substituted for other specimens. With regard to gas-charged specimens tested at f = 0.2 ~ 20 Hz, the lower the frequency, the shorter the fatigue lives in the area of finite life. On the other hand, fatigue limit of gas-charged smooth specimens tested at f = 500 Hz (C_H = 0.25 ~ 0.08 wppm) was not obviously different in comparison to that of uncharged smooth specimens.

The dashed line and the solid line in Figure 11 are predicted nondimensional S-N curves based on the fatigue crack growth properties under the following assumptions. The solid line is a predicted curve for uncharged specimens and the dashed line is a lower limit of a predicted curve for gas-charged specimens. Based on the predicted value of tensile strength, $\sigma_{UTS} \approx 934$ MPa, and the measured value of fatigue limit for hydrogen-charged and uncharged specimen, $\sigma_w \approx 350$ MPa, it can be considered that the predicted curves are effective in region of less or equal $\sigma_{UTS}/\sigma_w \approx 2.67$.

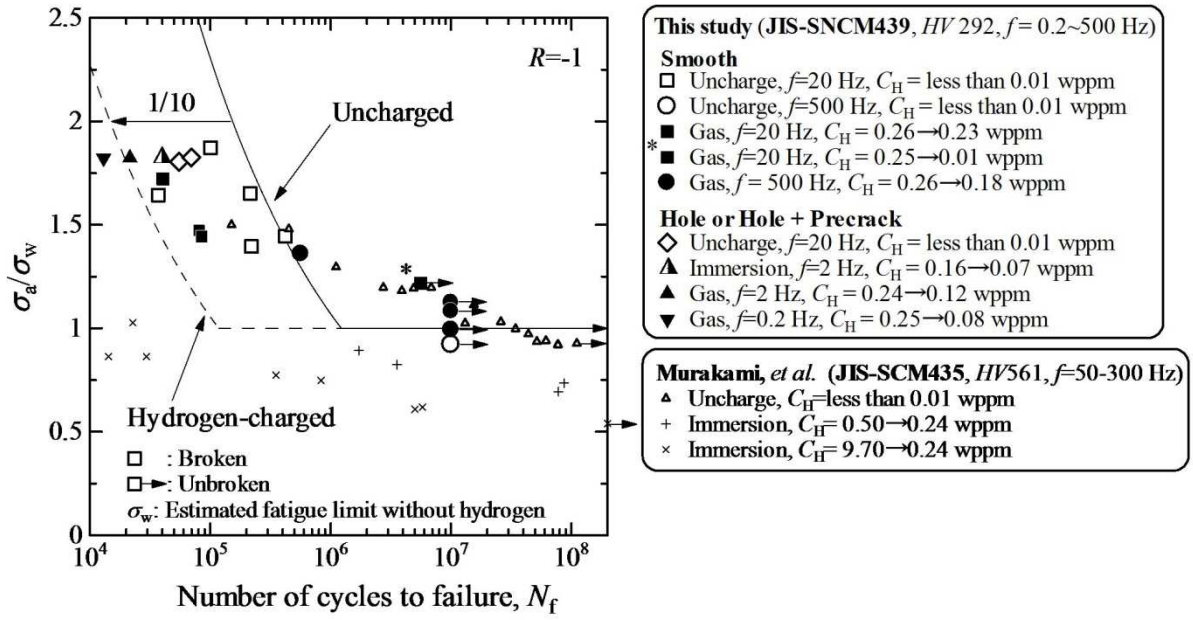

Figure 11. Modified S-N diagram constructed with the $\sqrt{area}$ parameter model.

Fatigue properties were calculated by assuming m in Figure 11 as m ≈ 3 and approximating da/dN-ΔK data. Then, constant value C for uncharged specimens is calculated as $C_u \approx 7.16 \times 10^{-13}$. Since the upper limit of hydrogen-induced fatigue crack acceleration is about 10 times, C for hydrogen-charged specimens is calculated as $C_{H(lim)} \approx 7.16 \times 10^{-12}$. The reason for assuming that m ≈ 3 is because the predicted curves become independent from the dimension of initial defect. Relation between fatigue life of uncharged specimens, NfU and that of hydrogen-charged specimens, is expressed as $N_{fH} \approx (1/10)\, N_{fU}$ because $C_{H(lim)} \approx 10\, C_u$.

The stress intensity factor range, ΔK, was calculated by assuming that fatigue crack propagates as semicircular crack [22]:

$$\Delta K = 0.71 \Delta\sigma \sqrt{\pi a} \qquad (8)$$

where a is the depth of semicircular crack. From the relationship of $\sqrt{\pi/2} \cdot a = \sqrt{area}$, Equation (8) becomes as the following:

$$\Delta K = 0.634 \Delta\sigma \sqrt{\pi \sqrt{area}} \qquad (9)$$

Fatigue propagation life, N_p, is obtained by integrating Equation (7) after substituting Equation (9) into Equation (7).

ISSN 1516-392X

$$N_p = \frac{2}{0.634^3 \pi^{3/2} C(\Delta\sigma)^3} \frac{1}{\left(\sqrt{area}_i\right)^{1/2}} \qquad (10)$$

In that integration, m is evaluated as m ≈ 3, and the dimension of the initial defect, $\sqrt{area}_i$, was assumed to be much smaller than the dimension of the final defect, $\sqrt{area}_f$. Given the relation of Δσ = 2σa, the $\sqrt{area}_i$ can be cancelled out from Equation (10) substituting Equation (9) into Equation (10) and following nondimensional S-N curve is derived.

$$\frac{\sigma_a}{\sigma_w} = \frac{1}{\alpha(HV+120)} \left(\frac{1}{4 \cdot 0.634^3 \pi^{3/2} C} \right)^{1/3} N_p^{-1/3} \qquad (11)$$

Since Equation (11) does not include the dimension of initial defect, $\sqrt{area}_i$, life prediction curve for uncharged specimens is shown as one solid line in Figure 10, substituting $C = C_u \approx 7.16 \times 10^{-13}$. Similarly, the dashed line in Figure 11 can be calculated as the lower limit of life prediction curve for gas-charged specimens by assigning $C = C_{H(lim)} \approx 7.16 \times 10^{-12}$. Where, α = 1.43 was substituted because crack is assumed to be surface semicircular crack. Also, fatigue limit or threshold stress intensity factor range of uncharged and gas-charged specimens was to consist at $\sigma_a/\sigma_w=1$. The results of uncharged and gas-charged specimens are plotted between the two life prediction curves.

In section 3.1, the maximum hydrogen content of storage cylinder of 70 MPa HS was estimated at approximately 0.33 wppm. Consequently, at this time, it is believed that the dashed line can be applied to fatigue design of storage cylinder of 70 MPa HS as the lower limit of S-N properties of gas-charged specimens that contain C_H=0.25 ~ 0.08 wppm hydrogen.

The dashed line shows that even for gas-charged specimen, infinite life design can be done in region of $\sigma_a/\sigma_w \leq 1$. It should be noted that if the cleanness of the material is improved, fatigue limit, σw, becomes larger. Then, the applicable stress amplitude will be improved. Although the dashed line can be used as the lower limit of S-N properties of gas-charged specimens that contain C_H=0.25 ~ 0.08 wppm hydrogen regardless of initial defect size, the cleanness of the material is also important factor to improve the safety of the storage cylinders.

Murakami and Nagata [23] conducted similar tension-compression fatigue tests of specimens of Cr-Mo steel (JIS-SNCM435, HV 561) with and without hydrogen at R = -1, f = 50 ~ 300 Hz at room temperature in laboratory air. Fracture origins of uncharged and hydrogen-charged specimens were internal Al_2O_3 inclusions ($\sqrt{area}$ = 15.7 ~ 72.6 μm, average $\sqrt{area}$ = 31.1 μm).

Figure 11 shows the results by Murakami et al.[23] in addition to results of this study. The JIS-SCM435 performed by Murakami et al. is harder (HV 561) compared to JIS-SNCM439 performed in this study (HV 292), and contains smaller inclusions than JIS-SNCM439 used in this study. However, the results of uncharged specimens by Murakami et al. almost agree with those of uncharged specimens performed in this study. This fact indicates that modified S-N diagram can eliminate the effect of the hardness of materials and also the effect of the dimensions of initial defect.

On the other hand, fatigue limit of hydrogen-charged specimens by Murakami et al. that contained $C_{H,R} \geq 0.50$ wppm hydrogen greatly decreased in comparison to that of hydrogen-charged specimens tested in this study. From this result, it would appear that the decreasing of fatigue limit due to hydrogen depends on material hardness (i.e. microstructure) and/or the hydrogen content of the material. It can be thought that fatigue limit will decrease at least when the material is a high strength steel and it contains $C_{H,R} \geq 0.50$ wppm hydrogen.

4 CONCLUSIONS

The effects of hydrogen on the fatigue properties of the Ni-Cr-Mo low alloy steel, JIS-SNCM439, which is a candidate material of storage cylinder of 70 MPa hydrogen station, were investigated. The conclusions can be summarized as the following:

(1) Fatigue lives of hydrogen-charged specimens decreased by 80 % when tested at f = 0.2 Hz, and 70 % when tested at f = 2 Hz with pre-charged hydrogen.

(2) Cluster of Al_2O_3 inclusions ($\sqrt{area} \approx$ 30 ~ 200 µm) existed at fracture origins of all smooth specimens. The larger the inclusion size, the lower the fatigue strength. Therefore, Ni-Cr-Mo steel of higher-cleanness compared to material used in this study is required to improve the safety of the storage cylinders.

(3) Fatigue crack growth rates, da/dN, were accelerated in the presence of hydrogen, and were strongly dependent on the test frequency. The lower the test frequency was, the more significant the acceleration. However, there is an upper limit of hydrogen-induced da/dN acceleration. The upper limit of the acceleration was approximately 10 times higher compared to da/dN of uncharged specimens in the presence of hydrogen content of 0.08 ~ 0.25 wppm.

(4) Fatigue limit was not obviously different between hydrogen-charged and uncharged specimens with the material (JIS-SNCM439, HV 292) and the testing conditions (R = -1, f = 500 Hz) in this study. This finding shall be further investigated.

(5) Considering the upper limit value of the acceleration of da/dN, the lower limit of modified S-N curve for hydrogen-charged specimen (hydrogen content: $C_H \leq 0.25$ wppm) was predicted. Life prediction and fatigue design of storage cylinder of hydrogen station can be possible based on the data obtained in this study when the dimension of initial defect or inclusion is estimated by applying statistics of extremes.

Acknowledgements

This research was supported by the NEDO Fundamental Research Project on Advanced Hydrogen Science (2006 to 2012).

REFERENCES

1 Japan Hydrogen & Fuel Cell Demonstration Project, website: http//www.jhfc.jp/ (accessed on 12/07/2009).

2 TANAKA, H. et al., Effect of Hydrogen and Frequency on Fatigue Behavior of SCM435 Steel for Storage Cylinder of Hydrogen Station, *Transactions of the Japan Society of Mechanical Engineers, Series A,* Vol. 73, No. 736 (2007), pp. 1358-1365.

3 MURAKAMI, Y. et al., Acceleration of superlong fatigue failure by hydrogen trapped by inclusions and elimination of conventional fatigue limit, *Tetsu-To-Hagane, Journal of the Iron and Steel Institute of Japan*, Vol. 86, No.11 (2000), pp. 777-783.
4 KIM, K. B., et al, Effect of Hydrogen Content on Hydrogen Embrittlement of SNCM 439 Steel in Artificial Seawater, *Journal of the Society of Materials Science, Japan*, Vol. 35, No. 397 (1986), pp. 1182-1188.
5 FUKAI, Y. et al., Hydrogen and Metal (in Japanese), 1998, Uchida Rokakuho, p. 28, 110.
6 TAKAI, K. and WATANUKI, R., Hydrogen in Trapping States Innocuous to Environmental Degradation of High-Strength Steel, *ISIJ International*, Vol. 43, No. 4 (2003), pp. 520-526.
7 MURAKAMI, Y., Quantitative Evaluation of Effects of Defects and Non-Metallic Inclusions on Fatigue Strength of Metals, *ISIJ,* Vol. 75, No. 8 (1989), pp. 1267-1277.
8 MURAKAMI, Y., Metal Fatigue: Effects of Small Defects and Nonmetallic Inclusions, 2002, Elsevier, p.93.
9 SHIRATORI, M. et al., Analysis of Stress Intensity Factors for Surface Cracks Subjected to Arbitrarily Distributed Surface Stresses, *Transactions of the Japan Society of mechanical Engineers, Series A*, Vol. 53, No. 488 (1986), pp. 779-785.
10 ASTM E 647 – 05: Standard Test Method for Measurement of Fatigue Crack Growth Rates, ASTM INTERNATIONAL 2005:45.
11 MATSUOKA, S. et al., Effect of hydrogen on the tensile properties of 900-MPa-class JIS-SCM435 low-alloy-steel for use in storage cylinder of hydrogen station*, Nippon Kinzoku Gakkaishi/Journal of the Japan Institute of Metals*, Vol. 70, No. 12 (2006), pp. 1002-1011.
12 National Institute for Materials Science, Japan, Fatigue Data Sheet No. 25, (1981).
13 MURAKAMI Y., and NAGATA, J., Elimination of Conventional Fatigue Limit due to Fatigue Crack Originated at Nonmetallic Inclusion, and Non-propagating Crack Originated at Artificial Small Hole, *Transactions of the Japan Society of Mechanical Engineers, Series A*, Vol. 72, No. 720 (2006), pp. 1123-1130.
14 FURUYA, Y. et al., Effects of Inclusion and ODA Sizes on Gigacycle Fatigue Properties of High-strength Steels, *Tetsu-to-Hagane*, Vol. 91, No. 8 (2005), pp. 630-638.
15 LIU, Y. B. et al., Dependence of Fatigue Strength on Inclusion Size for High–Strength Steels in Very High Cycle Fatigue regime, *Materials Science and Engineering A*, Vol. 517, (2009), pp. 180-184.
16 MURAKAMI, Y., and ENDO, M., Effects of Hardness and Crack Geometry on DKth of Small Cracks, *Journal of the Society of Materials Science, Japan*, Vol. 35, Nà. 395 (2004), pp. 911-917.
17 MURAKAMI, Y., and ENDO, M., Assessment Method for Effect of Small Defects on Fatigue Strength (in Japanese), *Transactions of Japan Society of Mechanical Engineers, Series A*, Vol. 49, No. 438 (1983), pp. 127-136.
18 PARIS, P. C., ERDOGAN, F., A Critical Analysis of Crack Propagation Laws, *Transactions of the ASME, Series D. Jornal of Basic Engineering*, v. 85, n. 64, 528-34, 1963.
19 KLESNIL M. and LUKInfluence of Strength and Stress History on Growth and Stabilisation of Fatigue Cracks, *Engineering Fracture Mechanics*, v. 4, (1972), p. 77-92.
20 MURAKAMI, Y., et al., Quantitative Evaluation of Effects of Nonmetallic Inclusions on Fatigue Strength of High Strength Steel, *Transactions of Japan Society of Mechanical Engineers, Series A*, Vol. 54, No. 500 (1988), pp. 688-696.
21 MURAKAMI, Y., and USUKI, H., Prediction of Fatigue Strength of High-Strength Steels Based on Statistical Evaluation of Inclusion Size, *Transactions of Japan Society of mechanical Engineers, Series A*, Vol. 55, No. 510 (1989), pp. 213-221.
22 MURAKAMI, Y., Ed., Stress Intensity Factors Handbook. Pergamon,1987. v. 2, p. 824.
23 MURAKAMI, Y., and NAGATA, J., Effect of Hydrogen on High Cycle Fatigue Failure of High Strength Steel, SNCM435*, Journal of the Society of Materials Science, Japan*, Vol. 54, No. 4 (2005), pp. 420-427.